EILERS GRADUATE STUDENT FELLOWSHIP
FINAL REPORT

EILERS FELLOW:	Feng Gao
FACULTY ADVISOR:	Prof. William A. Phillip
REPORT PERIOD:	12 months
PROJECT TITLE:	Elucidating the Role of Electrostatic Interactions in Facilitating Ion Transport through Charge-Mosaic Membranes for Water Purification and Desalination Applications
CONNECTION TO ND ENERGY'S RESEARCH AREAS (CHECK ALL THAT APPLY):	**(x) Energy Conversion and Efficiency** **( ) Sustainable and Secure Nuclear** **( ) Smart Storage and Distribution** **( ) Transformation Solar** **( ) Sustainable Bio/Fossil Fuels** **( ) Transformative Wind**

MAJOR GOALS AND ACCOMPLISHMENTS:
List your major research goals and provide a brief description of your accomplishments (1-2 sentences). Indicate the percentage completed for each goal. Please use a separate sheet to share additional details, technical results, charts, and graphics.

MAJOR RESEARCH GOALS	ACTUAL PERFORMANCE AND ACCOMPLISHMENTS	% OF GOAL COMPLETED
Fabricate charge-patterned mosaic membranes with varying surface pattern and experimentally connect surface pattern characteristics with ion transport properties of charge-mosaic membranes.	Charge-patterned mosaic membranes of varying surface patterns were fabricated systematically (Fig 1 and Fig 2). Such variations were encapsulated into a single variable, interfacial packing density (σ) which quantified the fraction of the membrane covered by interfacial junctions between oppositely-charged domains. As shown in Fig 3, transport of symmetric electrolytes (i.e., KCl, $MgSO_4$) increased with the value of σ, while σ did not affect the transport of asymmetric electrolytes (i.e., $MgCl_2$, K_2SO_4).	100%
Numerically elucidate the transport mechanism of symmetric and asymmetric salts through charge-patterned mosaic membranes.	Theory showed the salt partitioning at the membrane-solution interface determined the separation performance of the mosaics. Hence, the development of the membrane potential was solved at the interface of the mosaics (Fig 4 A-C). Based on the orientation of the electrical field lines, the membrane surface was sorted into regions that "interact only with ions in solution" and regions that "interact with other portions of the membrane". The former retarded the transport of salts while the latter facilitated the transport of the salts. This was indicated by the white and gray regions in Fig 4 D-F. As the interfacial packing density (σ) increased, the interfacial junctions between the oppositely charged domains increased which led to greater enrichment of symmetric salts. However, due to the strong electrostatic interaction between the divalent co-ions and the charge-functionalized domains, the concentrations of ions were skewed from their stoichiometric ratio which was the reason that the transport of asymmetric salts was not significantly affected by the pattern geometry (Fig 5).	100%
Understand how ion transport behavior is affected by solution composition as mixed salts systems are typically encountered in real-world applications such as hard water softening (Na^+, Mg^{2+}) and nutrient recovery (NO_3^-, PO_4^{3-}).	The ability of the charge-patterned mosaic membranes to promote the permeation of a symmetric salt and retard the permeation of an asymmetric salt was preserved in mixed salt solutions that contained equimolar amounts of KCl and $MgCl_2$ (Fig 6). This was indicated by the enrichment of KCl and rejection of $MgCl_2$ when the membrane was challenged by a mixed solution (Fig 6A). Furthermore, the separation of KCl and $MgCl_2$ was more distinct as the total ionic strength in the solution decreased (Fig 6B) which reinforced the role of electrostatic interactions in determining the ion transport behavior.	70%

RESEARCH OUTPUT:
Please provide detailed information below regarding any output resulting from your research project.

CATEGORY	INFORMATION
EXTERNAL PROPOSALS	(Sponsor, Project Title, PIs, Submission Date, Proposal Amount)

	Based on the preliminary results, a proposal was submitted to the Army Research Office. The principal investigator is Prof. William Phillip.
EXTERNAL AWARDS	(Sponsor, Project Title, PIs, Award Date, Award Amount) NA
JOURNAL ARTICLES	1. Interfacial Junctions Control Electrolyte Transport Through Charge-Patterned Membranes, submitted 2. Controlled Post-Assembly Functionalization of Nanoporous Copolymer Membranes Informed by Fourier Transform Infrared Spectroscopy, submitted
BOOKS AND CHAPTERS	(Book Title, Chapter Title, Authors, Submission Date, Publication Date, Volume #, Page #s) NA
PUBLIC PRESENTATIONS, SEMINARS, LECTURES	1. AIChE Annual Meeting, Pittsburgh, PA, 2018 (oral presentation & poster) 2. 2018 Notre Dame – Purdue Symposium on Soft Matter & Polymers and Poster Session, Notre Dame (poser) 3. Membranes: Materials and Processes, Gordon Research Conference (GRC), New London, NH, August 12th-17th, 2018 (poster) 4. Membranes: Materials and Processes, Gordon Research Seminar (GRS), New London, NH, August 11th-12th, 2018 (invited talk)
AWARDS, PRIZES, RECOGNITIONS	(Purpose, Title, Date Received) Outstanding Poster Presentation Award, Notre Dame – Purdue Symposium on Soft Matter & Polymers and Poster Session, Oct 2018.
INTERNAL COLLABORATIONS FOSTERED	(Collaborator Name, Organization, Purpose of Affiliation) Prof. Smith, Prof. Whitmer, and Prof. Chang
EXTERNAL COLLABORATIONS FOSTERED	(Collaborator Name, Organization, Purpose of Affiliation) NA
WEBSITE(S) FEATURING RESEARCH PROJECT	(URL) NA
OTHER PRODUCTS AND SERVICES (e.g., media reports, databases, software, models, curricula, instruments, education programs, outreach for ND Energy and other groups)	(Please describe each item in detail) NA

MAJOR GOALS AND ACCOMPLISHMENTS

(Additional Details, Technical Results, Charts and Graphics)

Project Summary

Membranes are utilized ubiquitously in natural and anthropogenic systems to control molecular transport (*1–3*). For example, in natural systems, the cell membrane separates the internal cellular milieu from the surrounding environment while helping to maintain homeostasis. In engineered systems, membranes are deployed to effect chemical separations (*4*), to generate and store energy (*5*), and to modulate the release of chemicals (*6*). Regardless of the membrane's function, developing a fundamental understanding of solute transport is critical to identifying molecular design strategies that guide the development of next-generation membranes. Significant effort has been dedicated to this endeavor, which has led to the fabrication of membranes that surpass the limitations of the permeability-selectivity trade-off (*7*, *8*). However, some design strategies remain underutilized and underexplored. For example, despite its prevalence in natural systems chemical patterning is not often utilized in engineered membrane platforms. Charge-patterned mosaic membranes, which consist of oppositely-charged domains dispersed across the membrane surface, are one example of a system where new phenomena emerge due to the patterned surface chemistry (*9*, *10*). If only positively-charged or negatively-charged functionality were utilized, the single-charge membrane would hinder the transport of dissolved salts through a Donnan exclusion mechanism (*11*). Conversely, charge mosaic membranes promote the transport of dissolved salts and can even concentrate salt in the membrane efflux (*12*). This unique characteristic has potential utility in numerous applications where the transport of ionic species needs to be controlled (*13*, *14*). Thus, myriad attempts have pursued the production of charge-patterned mosaic membranes. While some design strategies have been suggested by these efforts, the proliferation of charge mosaic membranes has been inhibited by complicated fabrication techniques that provided little control over nanoscale structure and chemistry. As a result, the molecular-level understanding of the phenomena that drive transport through charge-patterned membranes remains incomplete.

Here, we elucidate the molecular interactions that promote the transport of whole salts through charge-patterned membranes by systematically varying the pattern geometry and size. The effects of these parameters were encapsulated in a single variable, the interfacial packing density, σ, that quantified the fraction of the surface covered by junctions between oppositely-charged domains. Experimentally, the transport of symmetric electrolytes increased with the value of σ, while σ did not affect the transport of asymmetric electrolytes. Simulations demonstrate that for symmetric electrolytes, the structural charge heterogeneity reduces the barrier to ion partitioning promoting salt transport; while for asymmetric electrolytes, the charge heterogeneity skews the local availability of ions from their stoichiometric ratio hindering salt transport. These findings demonstrate the promise of accessing new transport mechanisms through chemical-patterning.

Figure

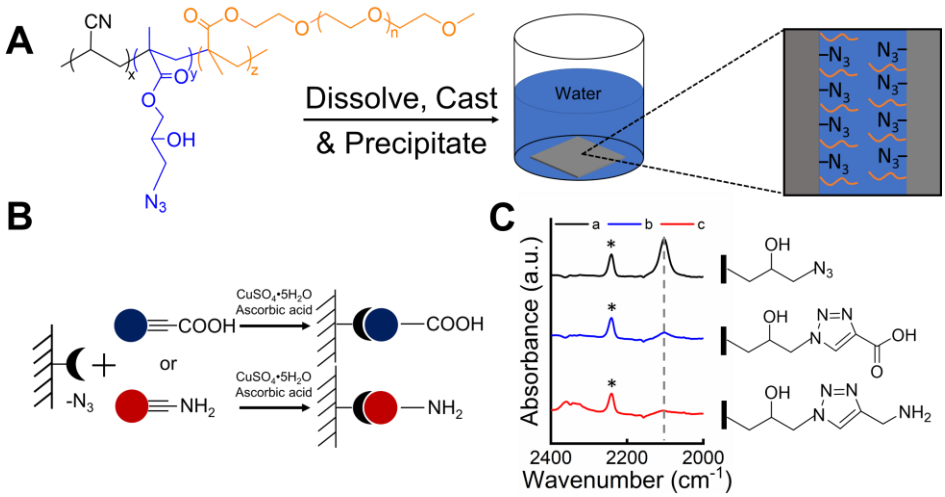

Fig. 1 Schematics of the fabrication and functionalization processes used to chemically-pattern nanostructured membranes. (**A**) The P(AN-OEGMA-AHPMA) copolymer was dissolved in a solvent to form a homogeneous solution that was then cast on a porous support to form the parent membranes. Due to the microphase separation of the copolymer, the pore walls of the parent membranes were lined with azido moieties. (**B**) The charge-functionalized domains of the mosaic membranes were formed through the copper(I)-catalyzed azide-alkyne cycloaddition (CuAAC) reaction. Reactive ink solutions containing alkyne-terminated molecules were dispensed onto the azido-functionalized substrate using an inkjet printer. In DI water, the propargyl amine-functionalized domains were positively charged as the amine moieties protonated to form ammonium groups. Conversely, the propiolic acid-functionalized domains were negatively charged since the carboxylic acid moieties deprotonated to form carboxylate groups. (**C**) The conversion of azide moieties was monitored using Fourier transform infrared spectroscopy. Specifically, the characteristic azide peak at ~2100 cm^{-1} was monitored before and after the parent azido-functionalized membrane (a) was functionalized with propiolic acid (b) or propargyl amine (c). The peaks marked with an * at ~2240 cm^{-1}, which are characteristic of the nitrile groups in the PAN matrix, were used to normalize the spectra.

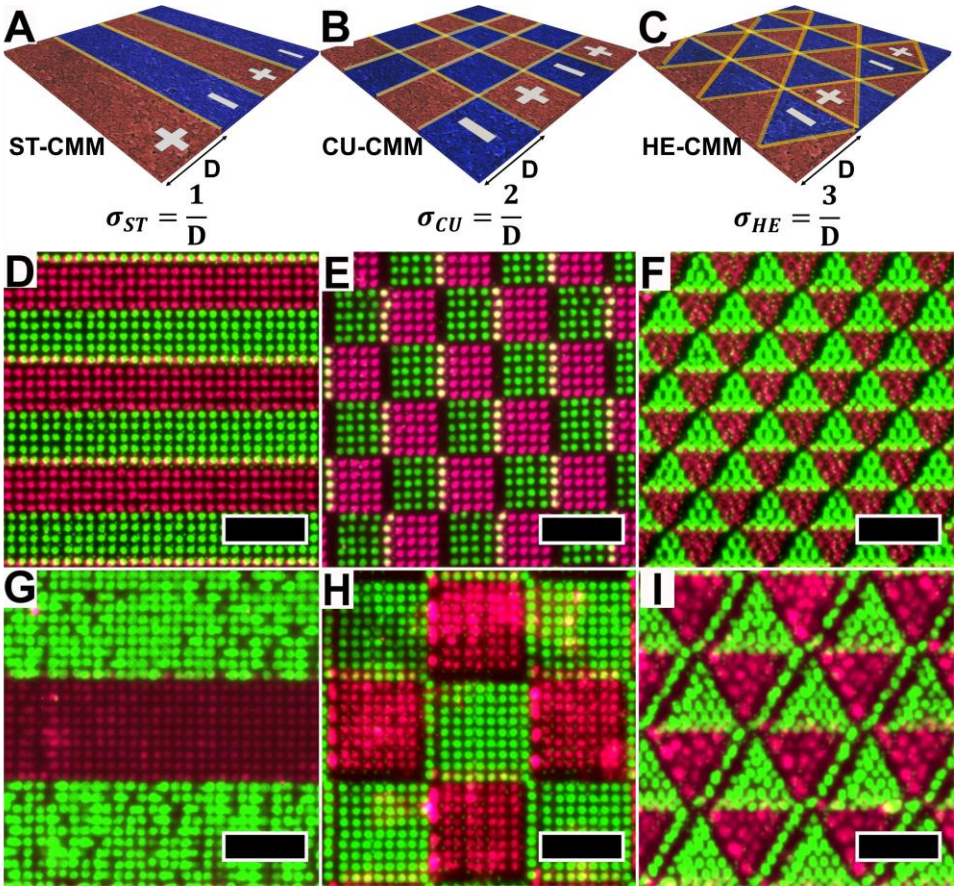

Fig. 2 The influence of pattern geometry and characteristic feature size, *D*, on the interfacial packing density, σ, of charge-patterned membranes. Schematics of (**A**) stripe-patterned (ST-CMM), (**B**) cubically-patterned (CU-CMM), and (**C**) hexagonally-patterned (HE-CMM) membranes. The interfacial junctions between oppositely-charged domains are highlighted in yellow. The interfacial packing density, which is defined as the total length of the interfacial junctions per unit area, can be calculated using the characteristic feature size, *D*. Fluorescent micrographs of stripe-patterned (**D** and **G**), cubically-patterned (**E** and **H**), and hexagonally-patterned (**F** and **I**) surfaces. The characteristic feature size was *D* = 300 μm in the middle row and *D* = 600 μm in the bottom row. Rhodamine 6G and sulfo-cyanine5 alkyne were added to the inks. A fluorescent microscope equipped with RFP and Cy5 light cubes was used to visualize the patterned domains. The domains containing Rhodamine 6G appear green and the domains containing sulfo-cyanine5 alkyne appear purple. Scale bars represent 500 μm.

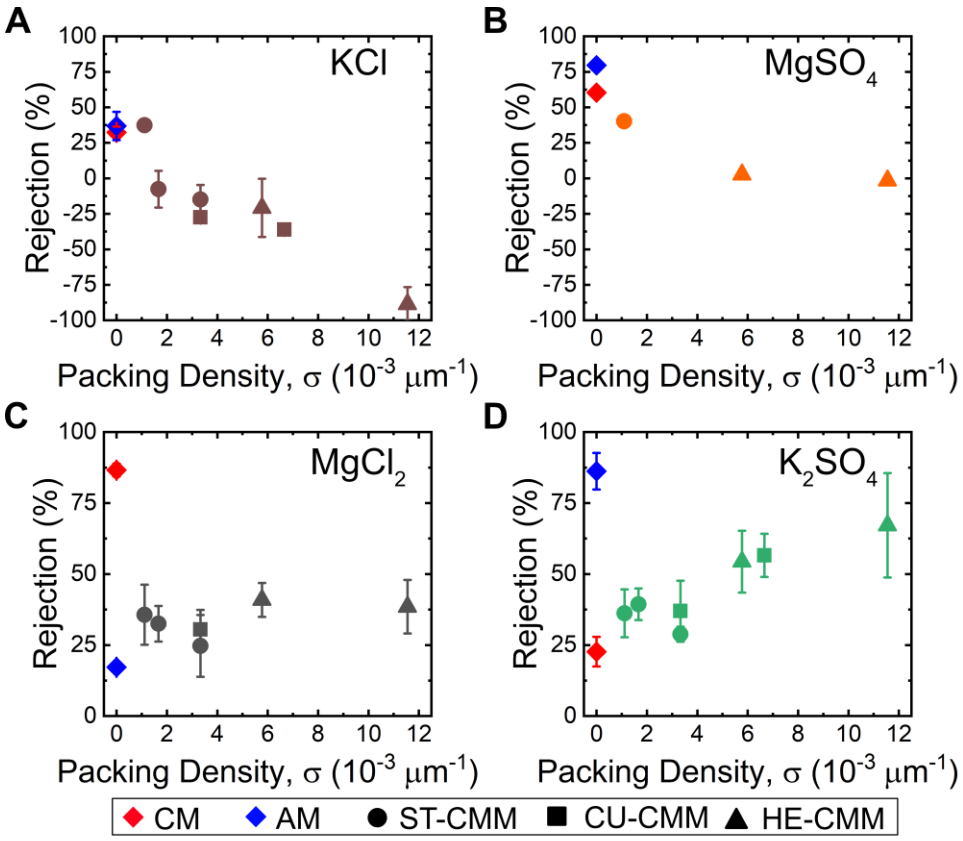

Fig. 3 Single salt rejection experiments conducted with single-charge control membranes and charge-patterned mosaic membranes of varying interfacial packing density. The single-charge membranes possessed all negative surface charge (anionic membranes, AM) or all positive surface charge (cationic membranes, CM). The charge-patterned mosaics possessed equal coverage of positively-charged and negatively-charged domains. Striped patterns (ST-CMM), cubic patterns (CU-CMM), and hexagonal patterns (HE-CMM) of varying characteristic feature sizes were printed to generate a range of interfacial packing density values. Results from feed solutions containing: (**A**) 100 μM potassium chloride (KCl). (**B**) 100 μM magnesium sulfate ($MgSO_4$). (**C**) 100 μM magnesium chloride ($MgCl_2$), and (**D**) 100 μM potassium sulfate (K_2SO_4). KCl and $MgCl_2$ rejection values were quantified using inductively coupled plasma optical emission spectroscopy (ICP-OES). K_2SO_4 and $MgSO_4$ rejection values were quantified using ion chromatography (IC). Solutes were dissolved in DI water. Error bar represents standard deviation which was calculated based on 4 permeate samples collected from two membranes of the same type.

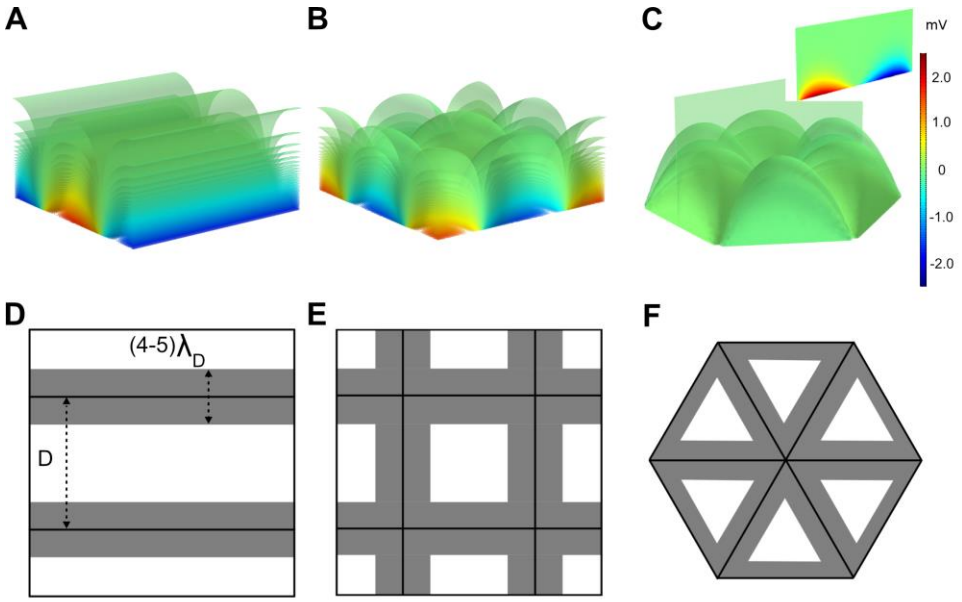

Fig. 4 The structural charge heterogeneity at the interfacial junctions of the charge-patterned membranes create regions that promote salt transport. Local variation in the electric potential near the membrane-solution interface (A-C). Each system consisted of a unit cell of the patterned membrane at bottom and a volume of solution above the membrane-solution interface. The cell was filled with an electrolyte solution at a concentration of 100 μM. The results shown are representative of the symmetric salt KCl. Top-down view of the three membrane unit cells indicating the regions of the membrane that "interact with other portions of the membrane" (grey) and the regions of the membrane that "interact only with ions in solution" (white) (D-F). If the angle between the membrane surface and the electric field line was greater than 88°, that area on the membrane was classified as interacting only with dissolved ions. Otherwise, it was said to interact with other portions of the membrane. The areas that interact with other portions of the membrane are centered at the interfacial junctions between oppositely-charged domains and cover a region with a width of ~4-5 Debye lengths (λ_D).

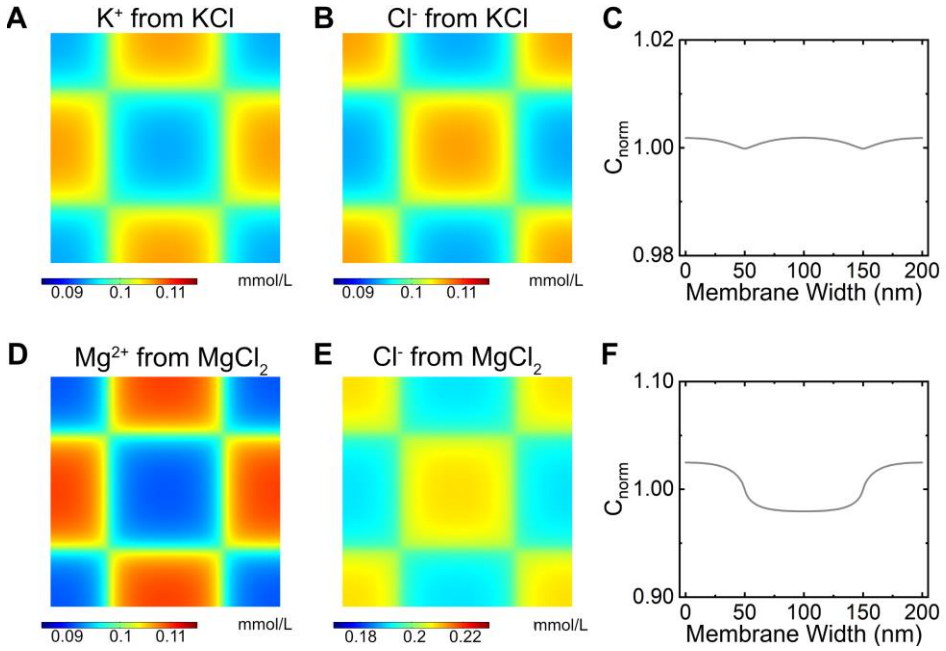

Fig. 5 The structural charge heterogeneity of the charge-patterned membrane surface modifies the local availability of ions for transport. Top-down view of concentration distribution of ions from dissolved KCl (**A, B**) and $MgCl_2$ (**D, E**). (**A**) K^+ (**B**) Cl^- (**D**) Mg^{2+} (**E**) Cl^-. Stoichiometry-normalized concentration of the salt, defined as

$$c_{norm}(\vec{r}) = \frac{\frac{c_1(\vec{r})}{|z_2|} + \frac{c_2(\vec{r})}{|z_1|}}{2c_b}$$

, was plotted for KCl (**C**) and $MgCl_2$ (**F**). In the expression above, c_1, z_1, c_2, and z_2 are the concentration and valence of the cation and the anion, respectively, and c_b is the salt concentration in solution. The values of the stoichiometry-normalized salt concentration presented were obtained from a horizontal line drawn through the midline of the membrane unit. The system consisted of a cubically-patterned mosaic surface with a feature size of 100 nm and a solute concentration of 100 μM. The square at the center of the pattern was positively charged.

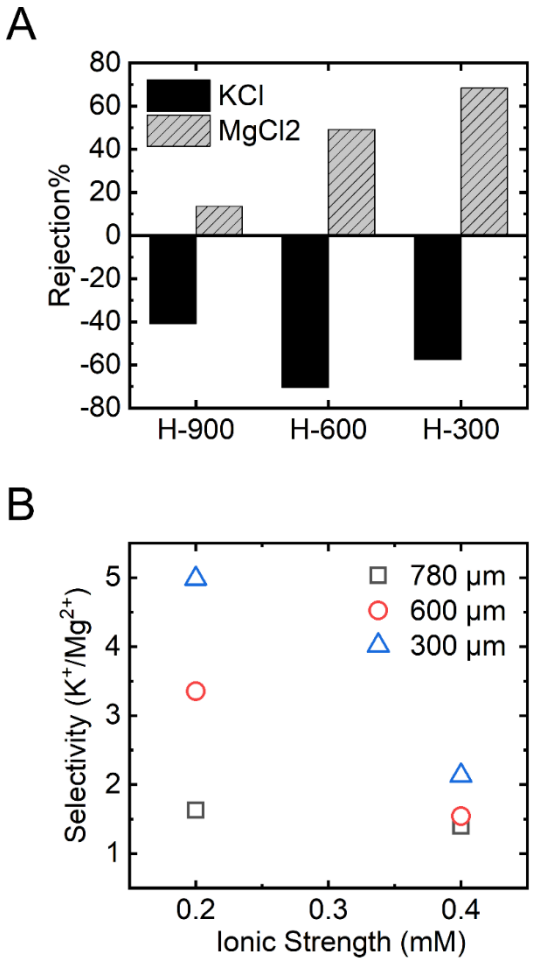

Fig. 6 Mixed salt separation performance of the charge-patterned membranes. A. Solute rejection of KCl and $MgCl_2$ from a mixture of two salts with total ionic strength of 200 µM. Hexagonally patterned mosaic membranes with feature size of 300 µm, 600 µm and 780 µm were used. The enrichment of K^+ and rejection of Mg^{2+} was consistent with results obtained from single solute rejection experiments. **B.** K^+/Mg^{2+} selectivity for a mixed salt feed solution. Aqueous solutions containing equimolar mixtures of KCl and $MgCl_2$ at ionic strengths of 200 µM and 400 µM were examined. Hexagonally-patterned charge mosaic membranes with feature sizes of 300 µm, 600 µm, and 780 µm were tested.

References

1. M. A. Shannon *et al.*, Science and technology for water purification in the coming decades. *Nature*. **452**, 301–310 (2008).
2. Y. X. Shen *et al.*, Achieving high permeability and enhanced selectivity for Angstrom-scale separations using artificial water channel membranes. *Nat. Commun.* **9**, 1–11 (2018).
3. T. Harayama, H. Riezman, Understanding the diversity of membrane lipid composition. *Nat. Rev. Mol. Cell Biol.* **19**, 281–296 (2018).
4. M. Elimelech, W. a Phillip, The future of seawater desalination: energy, technology, and the environment. *Science*. **333**, 712–717 (2011).
5. G. Merle, M. Wessling, K. Nijmeijer, Anion exchange membranes for alkaline fuel cells: A review. *J. Memb. Sci.* **377**, 1–35 (2011).
6. J. L. Weidman, R. A. Mulvenna, B. W. Boudouris, W. A. Phillip, Nanostructured Membranes from Triblock Polymer Precursors as High Capacity Copper Adsorbents. *Langmuir*. **31**, 11113–11123 (2015).
7. H. B. Park, J. Kamcev, L. M. Robeson, M. Elimelech, B. D. Freeman, Maximizing the right stuff: The trade-off between membrane permeability and selectivity. *Science (80-.).* **356**, 1138–1148 (2017).
8. J. R. Werber, A. Deshmukh, M. Elimelech, The Critical Need for Increased Selectivity, Not Increased Water Permeability, for Desalination Membranes. *Environ. Sci. Technol. Lett.* **3**, 112–120 (2016).
9. M. Higa, D. Masuda, E. Kobayashi, M. Nishimura, Charge mosaic membranes prepared from laminated structures of PVA-based charged layers 1 . Preparation and transport properties of charged mosaic membranes. *J. Memb. Sci.* **310**, 466–473 (2008).
10. P. Gao, A. Hunter, M. J. Summe, W. A. Phillip, A Method for the Efficient Fabrication of Multifunctional Mosaic Membranes by Inkjet Printing. *ACS Appl. Mater. Interfaces*. **8**, 19772–19779 (2016).
11. F. G. Donnan, The theory of membrane equilibrium. *Chem. Rev.* **1**, 73–90 (1924).
12. J. N. Weinstein, B. J. Bunow, S. R. Caplan, Transport properties of charged-mosaic membranes I. Theoretical models. *Desalination*. **11**, 341–377 (1972).
13. J. N. Weinstein, S. R. Caplan, Charge-mosaic membranes: dialytic separation of electrolytes from nonelectrolytes and amino acids. *Science*. **169**, 296–298 (1970).
14. T. Fujimoto, K. Ohkoshi, Y. Miyaki, M. Nagasawa, A New Charge-Mosaic Membrane from a Multiblock Copolymer. *Science*. **224**, 74–76 (1984).